International Journal of Applied Earth Observations and Geoinformation 102 (2021) 102369

Contents lists available at ScienceDirect

International Journal of Applied Earth Observations and Geoinformation

journal homepage: www.elsevier.com/locate/jag

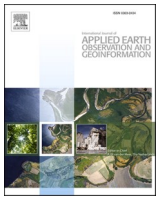

Ten years of volcanic activity at Mt Etna: High-resolution mapping and accurate quantification of the morphological changes by Pleiades and Lidar data

Marina Bisson [a,*], Claudia Spinetti [b], Daniele Andronico [c], Monica Palaseanu-Lovejoy [d], Maria Fabrizia Buongiorno [b], Oleg Alexandrov [e], Thomas Cecere [f]

[a] Istituto Nazionale di Geofisica e Vulcanologia, Sezione di Pisa, via Cesare Battisti 53, 56125 Pisa, Italy
[b] Istituto Nazionale di Geofisica e Vulcanologia, Sezione ONT, via di Vigna Murata, 00143 Roma, Italy
[c] Istituto Nazionale di Geofisica e Vulcanologia, Osservatorio Etneo, Sezione di Catania, Piazza Roma 2, 95125 Catania, Italy
[d] U.S. Geological Survey, Geology, Minerals, Energy and Geophysics Science Center, Sunrise Valley Dr., Reston, VA 20192, USA
[e] SGT Inc./NASA Ames Research Center, Intelligent Robotics Group M/S 269-3, Moffett Field, CA 94034, USA
[f] U.S. Geological Survey, National Land Imaging Program, Sunrise Valley Dr., Reston, VA 20192, USA

ARTICLE INFO

Keywords:
High resolution volcanic topography
Pleiades satellite
Airborne Lidar
Erupted volume
Mt. Etna

ABSTRACT

The topography of Mt. Etna, Italy, is subjected to continuous modifications depending on intensity and magnitude of eruptions that frequently occur at the volcano summit and flanks. In order to make high-resolution maps of morphological changes and accurately calculate the overall volume of the erupted products (e.g., lava flows, tephra fall out, scoriae cones) in ten years, we have compared the altimetry models of Mt. Etna derived from 2005 Airborne Laser Scanning data and 2015 Pleiades stereo satellite imagery. Both models cover a common area of 400 km^2 with spatial resolution of 2 m and comparable vertical accuracy (RMSE < 0.8 m). The results show that the area most affected by the erupted products is the mid-upper portion of the volcano with an altitude ranging from 1300 m to more than 3300 m a.s.l., value reached at the summit of the North East crater. In particular, this portion changes dramatically in the eastern sector due to the birth and growth of the New South-East Crater, the invasion of dozens of lava flows in the Valle del Bove, and the formation of the 2014 scoriae cones and lava field at the base of the North-East Crater. The total volume of products erupted in the investigated period results in 284.3±15.8 x 10^6 m^3 with a yearly average volume of 28.4 x 10^6 m^3/y comparable with the previous decades. In addition, the products emitted by the 2014 sub-terminal eruption are mapped and quantified including, for the first time, the volume of the 2014 scoriae cones generated on the eastern flank of North-East Crater This study demonstrates how a rigorous comparison between digital elevation models derived from different remote sensing techniques produce high accurate mapping and quantifications of morphological changes applicable for worldwide active volcanoes. This allows to quantify volumes and areas of erupted products reducing the error estimations, a crucial point to provide precise data often used as key parameters for many volcanic hazard studies.

1. Introduction

The Mt. Etna stratovolcano, located in the north-eastern area of Sicily (Italy), is one of the most active in the world (Branca and Del Carlo, 2004) and represents a potential hazard for about 900,000 people living on its slopes as well as hundreds of thousands of tourists who yearly visit the volcano (Andronico and Lodato, 2005). The volcanic activity of Mt. Etna, both explosive and effusive, has been particularly active and intense in the last 30 years (Barberi et al., 1993; Harris et al., 2011; 2012; Bonaccorso and Calvari, 2013; Proietti et al., 2020) causing continuous and consistent morphological changes of the volcano on its slopes and the summit area. Most of the morphological changes occurred during remarkable eruptions, which opened eruptive fissures on the flanks of the volcano and produced plentiful lava flow fields, as the

* Corresponding author.
E-mail addresses: marina.bisson@ingv.it (M. Bisson), claudia.spinetti@ingv.it (C. Spinetti), daniele.andronico@ingv.it (D. Andronico), mpal@usgs.gov (M. Palaseanu-Lovejoy), fabrizia.buongiorno@ingv.it (M. Fabrizia Buongiorno), oleg.alexandrov@nasa.gov (O. Alexandrov), tcecere@usgs.gov (T. Cecere).

https://doi.org/10.1016/j.jag.2021.102369
Received 2 August 2020; Received in revised form 14 May 2021; Accepted 14 May 2021
Available online 28 May 2021

1991–1993 (Calvari et al., 1994), 2004–05 (Del Negro et al., 2016; Fornaciai et al., 2021) and 2008–09 (Aloisi et al., 2009; Bonaccorso et al., 2011) eruptions. Large scoriae cones were also produced in 2001 (Calvari and Pinkerton, 2004) and 2002–2003 (Andronico et al., 2005). With more than 200 paroxysms (hereafter also named paroxysmal episodes; e.g., Andronico al., 2009a,b; 2014a; Behncke et al., 2014; De Beni et al., 2015; Andronico et al., 2015; 2016; Corsaro et al., 2017), the eruptive activity occurred in the summit area caused the rapid growth of craters, proximal coarse-grained tephra fallout, ash and lapilli dispersal in several distal areas, and the spreading of extensive lava flows, most of them in the eastern part of the volcano.

In literature, the mapping and volume quantifications of the Etna morphological changes are often referred to single eruptive events and estimated by the following methodologies: i) extrapolations from field data and modelling (Coltelli et al., 2007; Andronico et al., 2008); ii) estimations obtained by thermal remote sensing techniques (Harris et al. 1997; 1998; Bailey et al., 2006; Lombardo et al., 2011); iii) comparison between Digital Elevation Models (DEMs) before and immediately after the eruptive event (Neri et al., 2008; De Beni et al., 2019; Proietti et al., 2020). The first method, requiring proper collection of field data, depends on the accessibility and the extent of the erupted deposits. In different conditions, the other two methods (ii, iii) represent a valid solution for providing volume estimations, especially if the uncertainty is provided. This is still an open issue for the thermal satellite technique that, based on several parameters, suffers from multiple sources of uncertainty (Ganci et al., 2018; Lombardo et al., 2020). Conversely, the DEMs comparison method allows to correctly quantify the uncertainty, if the errors in x, y and z of source data used to produce the DEMs are quantified. In particular, multi-temporal topographic changes are detected by remote sensing derived DEMs elevation differencing, a conceptually simple approach to produce a 3D differential surface that can measure the spatial distribution of volume change (Etzelmuller, 2000). The derived DEMs have different qualities inherited from their original data source, pre- and post-processing techniques, filtering and interpolation procedures. These different characteristics result in inherited uncertainty that must be understood and propagated in comparisons of elevation data over broad temporal scales to ensure that observed elevation changes are meaningful (Anderson, 2018). For this reason, it is necessary that the source data are properly processed, and the derived products are compared following rigorous criteria based on fundamental rules of the spatial analysis: co-registration, same spatial resolution, comparable accuracy. These criteria assure that the methodologies take into consideration data source errors, source data variations, and error propagation. This last factor is important, since the access to 3D data are increasing with the wider availability of Lidar, stereo photogrammetry from commercial satellite imagery, and with the low-cost and accessibility of structure-from-motion derived elevation data.

In this study, an accurate identification and quantification of the overall Etna morphological changes are obtained by applying the third methodology previously mentioned. In detail, we compare two altimetry models of the volcano, the first derived from the 2005 Airborne Laser Scanning (ALS), the second obtained from the 2015 Pleiades stereo satellite imagery using the Structure from Motion (SfM) technique. Both models have a spatial resolution of 2 m and vertical root mean square error (RMSE) of 0.24 m and 0.78 m, respectively. Taking into account the extent of the two DEMs, a common area of 72 km^2, centred on the volcano summit, represents our study area (Fig. 1). This paper initially presents the two altimetry models and the recent volcanic activity. In the following, it describes the resulting map in terms of thickness and volume. Then a discussion of the results is presented, including some considerations on the drainage network and the roughness surface. Lastly, the conclusions resume the main remarks pointing out some possible hazard implications.

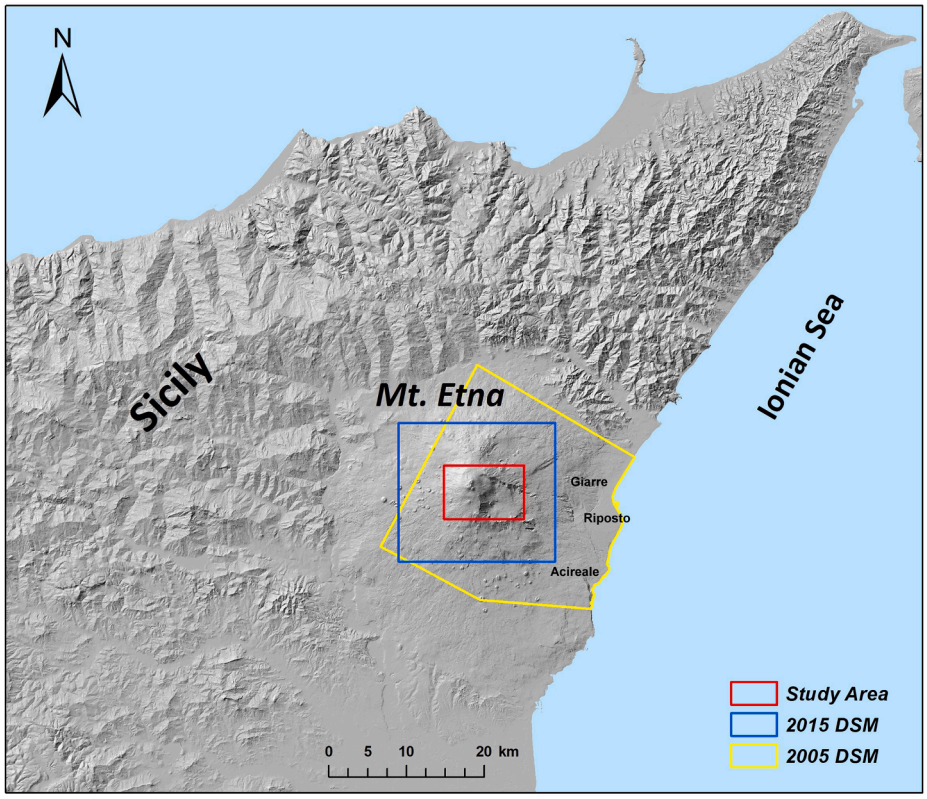

Fig. 1. Geographic setting of the investigated area. The 3 coloured outlines indicate the extent of Lidar DEM (yellow), the Pleiades DEM (blue) and the Study Area (red).

2. The 2005 ALS DEM

During the Airborne Laser Scanning (Axelsson, 1999) 2005 survey (September 29–30, 2005), 250 million points were acquired and processed to obtain a Digital Terrain Model (DTM) and a Digital Surface Model (DSM) of Mt. Etna at a spatial resolution of 2 m and vertical RMSE of ± 24 cm (Bisson et al., 2016). Both models, geo-coded into WGS84 UTM 33 N geodetic cartographic system, reproduce the topography of the volcano (Fig. 1) covering an area of 620 km^2 with an elevation ranging from 0 to 3300 m a.s.l. These models represent the most extensive high-resolution topographies of Mt. Etna to date and were validated with ground control points (GCP) selected from the Mt. Etna geodetic network (Bisson et al., 2016; Bonforte and Puglisi, 2006). Fig. 2a shows the 2005 morphology of the study area.

3. The 2015 Pleiades DEM

The Stereo Satellite Photogrammetry technique, using two or more images in stereo mode and standard procedures of processing (Deilami and Hashim, 2011), allows the reconstruction of DEMs with spatial resolution and accuracy depending on the sensor characteristics and the processed band. The 2015 Pleiades DEM was obtained by processing the pan-sharpened multispectral stereo imagery acquired on July 28, 2015 by the polar orbiting P-1A and P-1B satellites with an angle incidence of 16°. In detail, the pan-sharpened band 1 image (0.43–0.55 μm) at 1 m resolution was processed by using the NASA Ames Stereo Pipeline (ASP) procedure (Beyer et al., 2018). The ASP standard workflow was modified setting the best feature matching algorithm and introducing the conversion in *ortho*-metric heights in order to obtain a DSM comparable in spatial resolution and accuracy with the model of 2005 DEM

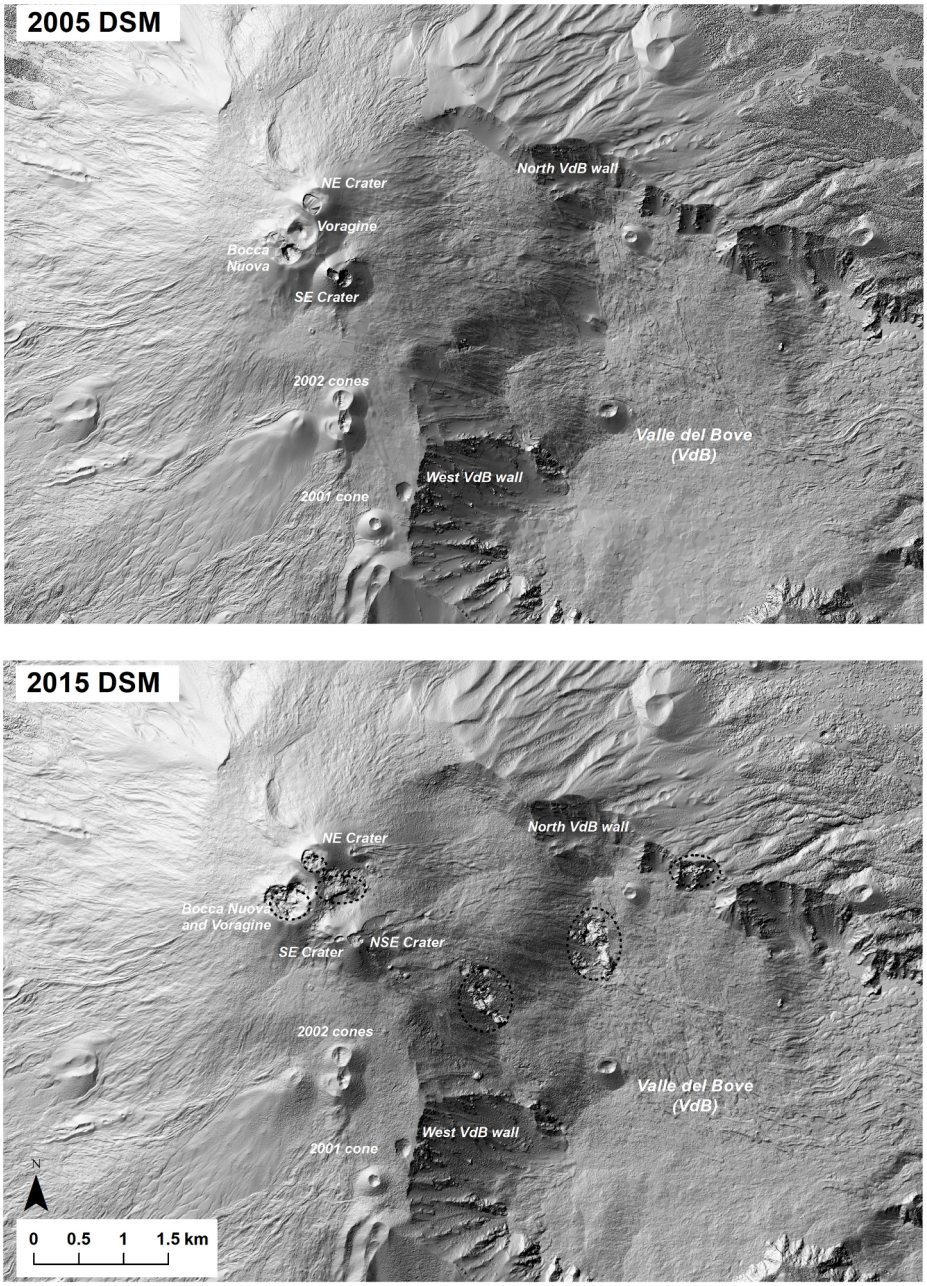

Fig. 2. The shaded relief of 2005 and 2015 DEMs, coming from ALS survey and Pleiades satellite data, respectively. The black dashed circles enclose false morphologies generated by the presence of meteorological clouds, fumaroles and volcanic plume as documented by the panchromatic band of the Pleiades data showed in Fig. 4.

(Palaseanu-Lovejoy et al., 2019). The Pleiades DEM, in *ortho*-metric height, has a spatial resolution of 2 m and covers 400 km^2 with elevation ranging from 382.2 m a.s.l. to 3326.5 m a.s.l., i.e., up to the summit area of Mt. Etna (Fig. 1). The model has an overall vertical RMSE of ± 78 cm and ± 50 cm in non-vegetated stable areas at elevation higher than 1800 m a.s.l. (Palaseanu-Lovejoy et al., 2019). Fig. 2b shows the 2015 morphology of the study area.

4. The recent volcanic history of Mt. Etna

Mt. Etna summit area includes five craters named North-East Crater (NEC), Voragine (VOR), Bocca Nuova (BN), South-East Crater (SEC), the most active crater of Mt. Etna since 1998, and New South-East Crater (NSEC) (Fig. 2b). The latter is the youngest cone, which gradually began to grow after 2011 over a lateral pit-crater located on the east flank of the SEC until they merged (Andronico et al., 2018a, 2018b). The NSEC overlooks the edge of the Valle del Bove (VdB) that extends towards the eastern side of the volcano (Fig. 2b). The large structure formed by the coalescence of the SEC with the NSEC constantly evolves due to the continuous eruptive activity. Hereafter, we use the term SEC-NSEC structure to indicate the composite cone made up of the merging of the two previous cones.

In the last 50–60 years, the eruptive history of Mt. Etna showed marked increasing activity in the number of eruptions and volume of erupted magma compared to the past centuries (e.g., Andronico and Lodato, 2005; Branca and Del Carlo, 2005) and, after 1995, the eruptive style was frequently characterized by explosive activity, although coeval or alternating with lava effusions. More than 200 paroxysmal episodes have been recorded since 1989. A few lava overflows and lava outputs from eruptive fissures have broken the slopes of the cones at the summit craters. The last paroxysmal episode occurred on 31 March-1 April 2021. After 2000 the upper flanks were affected by two long-lasting explosive/effusive eruptions in 2001 and 2002–2003 (Behncke and Neri, 2003; Andronico et al., 2005 and 2008), and prolonged effusive eruptions in 2004–05 (Del Negro et al., 2016), 2006 (Lombardo et al., 2011) and 2008–09 (e.g., Aloisi et al., 2009; Bonaccorso et al., 2011). The most recent flank eruption occurred on 24–27 December 2018, when an eruptive fissure opened at the base of the NSEC generated a copious lava output and, a poor tephra emission (Cannavò et al., 2019; Laiolo et al., 2019).

4.1. The 2005 – 2015 volcanic activity

In the following, we give an overview of the 2005–2015 eruptive activity characterizing the summit portion and the flanks of the volcano with the aim to summarize the volume of erupted products coming from field survey and available literature. Such volume will be compared with the volume value calculated by the methodology used in this work.

In the summit portion, the most frequent activity consisted of paroxysmal episodes, defined here as short eruptions with overall duration spans from few hours to few days. They are initially characterised by a resumption phase (Alparone et al., 2003), during which weak, discontinuous Strombolian explosions may be accompanied by a poor-fed lava output. Such explosions gradually increase more and more in frequency and intensity up to evolving into powerful Strombolian activity and/or lava fountaining. This is the paroxysmal phase, commonly lasting from tens of minutes to few hours and generates an unique formation of eruption column, sometimes up to 10 km above the crater, as well as fast coeval spreading of highly fed lava flows (e.g., Andronico et al., 2015; Corsaro et al., 2017). Typically, at Mt. Etna, these eruption columns cause proximal tephra fallout (<2 km) and distal tephra that reach over tens to hundreds of km away from the vent (Andronico et al., 2014). The conclusive phase sees the quick waning of the eruptive phenomena until their total (or almost complete) exhaustion.

In detail, there are 77 paroxysms recorded from 2005 to 2015, 26 of those from the SEC and 51 from the NSEC. In the considered period, we observed a wide intensity range of paroxysms, from small-to large-scale, during which the volume of distal tephra generated by the eruption cloud can vary widely (0.1–1)x 10^6 m^3 (Andronico et al., 2015). Such range of volumes is obtained considering few of 77 paroxysms since the distal tephra emitted by the most of those paroxysms is not estimated in terms of volumes in literature. Finally, although the dominant winds blowing above Mt. Etna disperse most of the tephra fallouts towards E and SE, a recent study on the 12–13 January 2011 lava fountain highlighted that 60% of the total erupted distal tephra fell within a radius of 5–6 km from the respective vent (Andronico et al., 2014).

As regards the lava flows emitted in all the paroxysmal episodes, the volumes are characterized by the same order of magnitude. In fact, the maximum length of these lava flows usually does not exceed 4.3 km from the vent, and most of them stop within 2–3 km, corresponding to volumes of (1–2)x 10^6 m^3 and altitudes of around 1900–2100 m a.s.l. (Behncke et al., 2014; De Beni et al., 2015).

In addition, the summit area is affected with less frequency to sub-terminal eruptions represented by volcanic activity from eruptive fissures which opened in close spatial and structural relation with the summit cones, i.e. over their slopes or at their foot. On 22 January 2014 a minor effusive activity began when lava was emitted from vents opened in the lower eastern flank of the NSEC. This activity went on with large fluctuations in the effusive rate for about 75 days, with the total lava volume estimated at 7.8 x10^6 m^3 (De Beni et al., 2015). Conversely, a larger sub-terminal activity affected the lower eastern flank of the NEC, where on 5 July 2014 an eruptive fissure system opened at ~ 3000 m (Spina et al., 2017). This eruption lasted around a month, producing simultaneously explosive activity associated with the formation of scoriae cones at the upper tips of the fissures, and lava output which formed a lava flow field down the northern wall of the VdB. The volume of this lava flow field was estimated in 5.9 x10^6 m^3 (De Beni et al., 2015).

With regard to the flank activity, only a single eruption is recorded in 2005–2015. It occurred on 13 May 2008, when a system of eruptive fissures, propagating from the base of the SEC toward the western wall of the VdB, started a prolonged effusive activity, which stopped on 6 July 2009 (Aloisi et al., 2009). The 2008–2009 flank eruption has produced lavas with an estimated volume around ~ 74 x10^6 m^3 (Behncke et al., 2016).

The main characteristics of Mt. Etna summit and flank activities are summarized in Table 1 reporting the volumes of erupted deposits (lava and proximal tephra) that are published in the literature. The Table highlights that most of lava flows are estimated in terms of volume, whereas the proximal tephra emitted during the paroxysmal episodes are not estimated except for the 2011–2012 and 2013 proximal tephra. The total volume resulting from data published in the literature is equal to ~ 218.81 x10^6 m^3, that is evidently underestimated.

5. Results and discussion

5.1. 2005–2015 morphological changes

The co-registration, the same spatial resolution (2 m) and the similar vertical RMSE (<0.8 m) allowed a rigorous comparison between the 2005 and 2015 DEMs in the common area. This study focuses on the area defined in Fig. 1 centred on the summit area and covering 72 km^2 with sides of 10 km by 7.2 km. Working on a GIS platform (ESRI environment), the map of difference in height (Fig. 3) was obtained by subtracting DEM2005 from the DEM2015. In this map, zones outlined in black have been excluded by the analysis as they show false values due to the presence of meteorological clouds, fumaroles and volcanic plume as documented by the panchromatic band of Pleiades data (Fig. 4). The values of the map range from −80 m to about +210 m and the error in elevation is calculated as RMSE of the differenced DSMs according to equation (1) below:

Table 1
Summary of Mt. Etna summit and flank activities from 2005 to 2015. The references are the main publications or internal reports dealing with the indicated eruptions. When published, the values of volumes are reported. The NEC = North-East Crater; NSEC = New South-East Crater; SEC = South-East Crater; VdB = Valle del Bove.

Year	Date	Type of activity	Vent location	Erupted volume estimation $10^6 m^3$		References
				lava	*proximal tephra*	
2006	15–24 July	Strombolian activity and Lava flow	SEC	2		Harris et al., 2011Andronico et al., 2009b
	13 September – 27 November	16 paroxysmal episodes	SEC	37		Andronico et al., 2009a,b; Harris et al., 2011
2007	29 March – 23 November	6 paroxysmal episodes	SEC			Andronico et al., 2009a,b;
2008	10 May	paroxysmal episode	SEC			Di Grazia et al., 2009
2008–2009	13 May 2008–6 July 2009	paroxysmal episode followed by flank eruption	SEC and W wall of the VdB	74		Di Grazia et al. 2009; Behncke et al., 2016
2011–2012	12 January 2011–24 April 2012	25 paroxysmal episodes	NSEC	28	19	Behncke et al., 2014; Andronico et al., 2014
2013	19 February – 28 December	21 paroxysmal episodes	NSEC	19.73	20.48	De Beni et al., 2015; Andronico et al., 2018a
2014	22 January – 7 April	subterminal eruption	NSEC	7.8		De Beni et al., 2015
	14–16 June	paroxysmal episode	NSEC	2.3		De Beni et al., 2015
	5 July – 10 August	subterminal eruption	base of the NEC	5.9		De Beni et al., 2015
	8–16 August	paroxysmal episode	NSEC	2.6		De Beni et al., 2015
	28 December	paroxysmal episode	NSEC			INGV-OE, 2014
2015	31 January – 15 May	3 paroxysmal episodes	NSEC			INGV-OE, 2015a,b
Partial volumes				179.33	39.48	
Total volume					218.81	

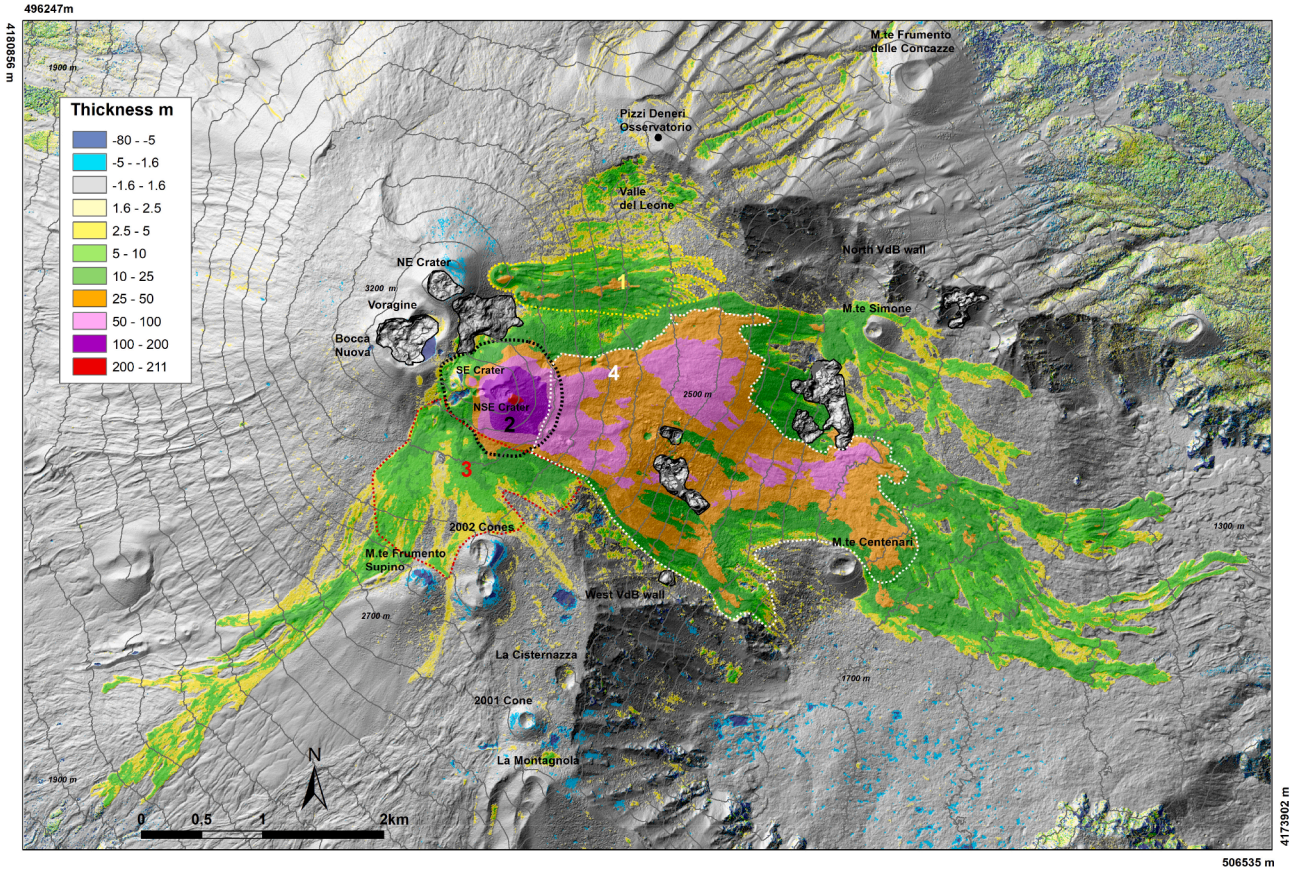

Fig. 3. Map of the difference in height 2005–2015 obtained comparing the Lidar and Pleiades altimetry models. The numbers 1, 2 3, and 4 indicate the four areas mostly affected by morphological changes from 2005 to 2015. The coordinates at the corners are expressed in meters according to the WGS 84 UTM N 33 Cartographic System.

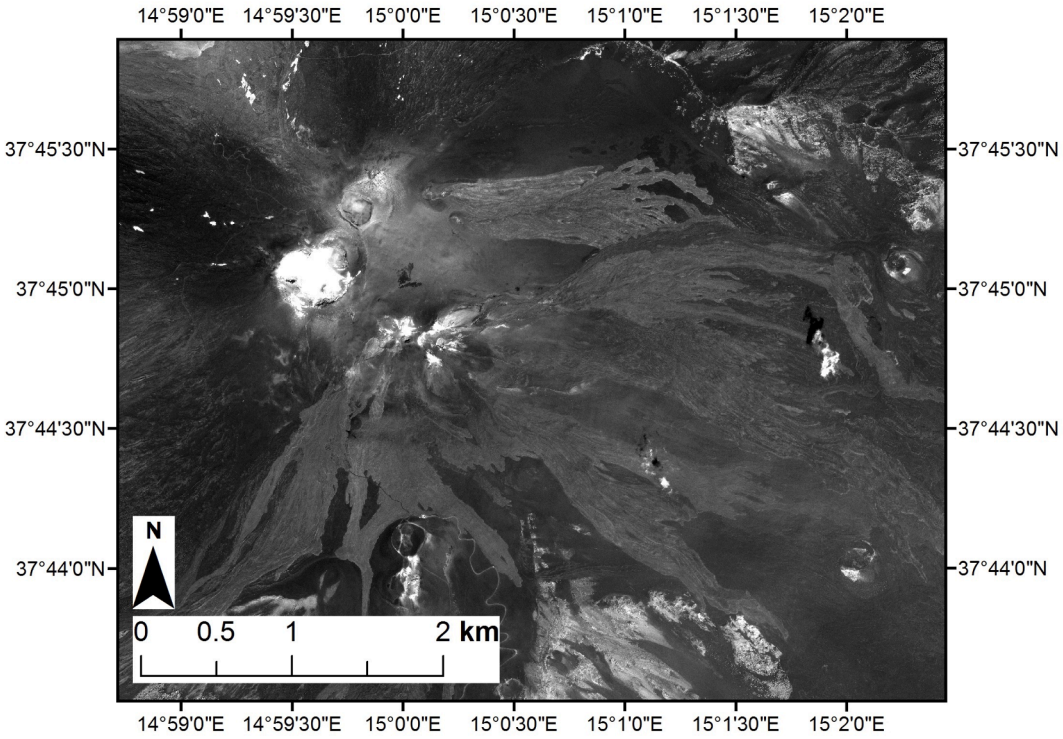

Fig. 4. Image of panchromatic band of Pleiades data acquired on July 28, 2015.

$$RMSE_{dif} = \sqrt{RMSE_{ALS}^2 + RMSE_{SfM}^2} \quad (1)$$

where $RMSE_{dif}$ represent the RMSE of the result, $RMSE_{ALS}^2$ represents the RMSE of the Lidar data, and $RMSE_{SfM}^2$ represents the RMSE of the Pleiades derived data.

The accuracy of the result at 68% confidence interval (C.I.) (for 1 Standard Deviation) is ± 0.82 m, and for 95% C.I. is ± 1.6 m (2 Standard Deviation).

In Fig. 3, the coloured areas identify zones affected by real morphological changes, because the map values are greater than +1.6 m and lesser than –1.6 m. The areas with values between –1.6 m and +1.6 m are visualized by grey tones of the shaded relief and identify zones where it is not possible to distinguish accumulations of deposit from losses of material or unchanged surface. The positive and negative values in the map have distinct origin and interpretations. The positive values represent the cumulative thickness of the erupted products in the 10 years and are visualized with a colour ramp from yellow to red through the green, orange, pink and purple tones. In particular, the lowest thicknesses (<2.5 m) are in light yellow and identify some branches of lava flows or portions of pyroclastic material deposited in specific zones such as Valle del Leone or the canyons situated between the Pizzi Deneri Osservatorio and Mt. Frumento delle Concazze, both located in the north-east direction to the upper summit. Instead, the highest thicknesses (greater than 200 m) are coloured in red and identify the summit portion of the NSEC.

The negative values indicate areas affected by decreases in elevation and are coloured with blue tones. The light blue colour identifies the areas where the difference in height reaches −5 m, whereas dark blue discriminate zones affected by greater decreases (from −5 m to −80 m). In particular, the minimum value of −80 m is only present in the south-east crater rim of Bocca Nuova that collapsed in the investigated period. Further blue areas are well recognizable over or at the base of the 2001 and 2002–2003 cones, in a sector of the NEC, in some portions of the NNE flank of the NEC and, finally, in some very small areas in the western sector of Valle del Bove. Such areas are the result of probable erosion or detachment phenomena.

5.2. Spatial analysis of morphological changes

The 2005–2015 eruptive activities in Valle del Bove are characterized by the spatial distribution of positive values in the difference map (Fig. 3). In particular, there is a central area located between 1750 m and 3250 m a.s.l. (orange colour) where the minimum retrieved thickness is 25 m. Inside this area, three sub-areas are well identified thanks to the thickness ranging from 50 m to 100 m (pink colour). These high thicknesses are the result of the overlapping of numerous lava flows occurred between September 2005 and July 2015, not distinguishable between them but evaluable at least in over 50 lava flows (references in Table 1). Another zone characterised by elevate thicknesses is represented by the cone-shaped structure generated by the intense activities of the SEC and NSEC cones (purple colour in Fig. 3), where the highest value of 210.7±1.6 m is reached on the rim of the NSEC. Thicknesses greater than 25 m are reached by the lavas present only in the Valle del Bove, whereas thicknesses lower than 10 m affect both the Valle del Bove and the South-West flank and stop at elevations around 1300 m and 1900 m a.s.l., respectively. Zones with moderate thicknesses (from 3 m to 10 m), are well recognizable in Valle del Leone and in some of the canyons situated between the Pizzi Deneri Observatory and Mt. Frumento delle Concazze, both located to the NE of the summit portion of the volcano (Fig. 3). The presence of these moderate thicknesses is probably due to coarse-grained tephra deposits produced by powerful lava fountains in 2013 (Poret et al., 2018) that, subsequently were eroded by intense rains and/or snow melting, and accumulated along natural and radial drainage routes present in the canyon to the SW of Mt. Frumento delle Concazze and in some portions of Valle del Leone walls. These drainage routes (Bisson et al., 2019) are also shown in Fig. 5 where they are combined with the map of the difference in height. In detail, Fig. 6a shows the radial canyons upstream of Mt. Frumento delle Concazze internally filled by layers of tephra that were removed from uneven ridges or gravity-slid from the steep sidewalls. Furthermore, in the centre of the canyons, the superficial and temporary drainage caused by rain is well marked (Fig. 6a), resulting in thick piles of tephra deposits on small areas where break-in-slopes are present. The limited depression

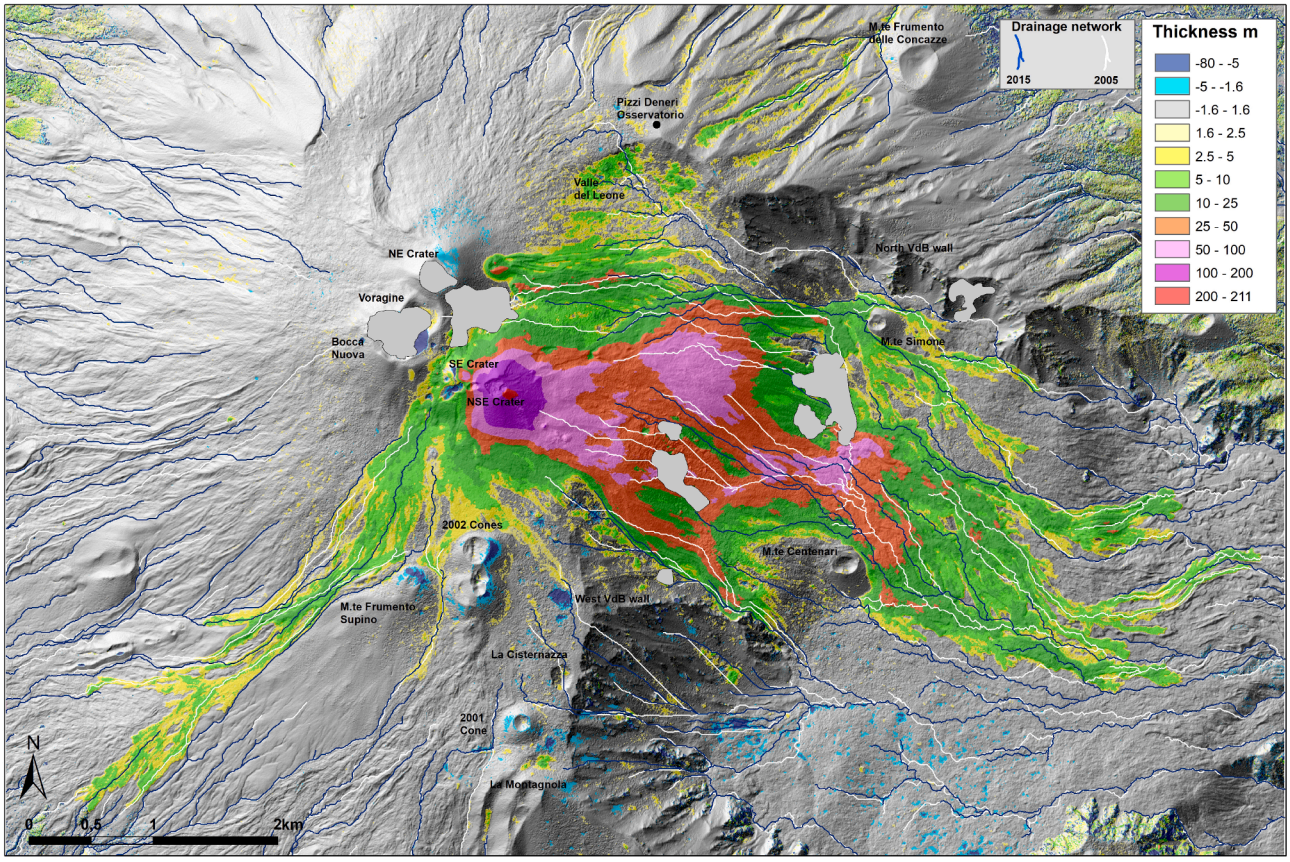

Fig. 5. The 2005 and 2015 drainage networks at Mt. Etna. The zones in grey enclose the false morphologies generated by the presence of meteorological clouds, fumaroles and volcanic plume.

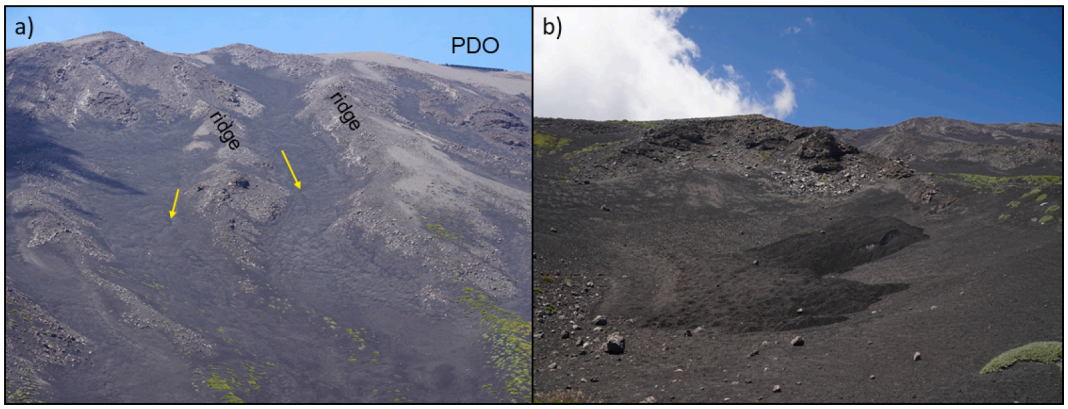

Fig. 6. a) Panoramic view of the NE area of Etna between Pizzi Deneri Osservatorio (PDO; the building in the top-right of the volcano) and Mt. Frumento delle Concazze (from which the picture is taken). The yellow arrows show the shallow drainage in the middle of the canyons. b) Small lobes due to solifluction processes in the upper areas of Valle del Bove. Photos by D. Andronico.

areas close to Valle del Leone are also shaped by freeze and thaw cycle that, in general, at 1500–3000 m of altitude can be active for several months a year. The water that freezes in the ground increases in volume and exerts significant pressure in the thick tephra cover where it has penetrated, fragmenting, and displacing the volcanic material that can be removed and transported downwards more easily by rain. In other cases, solifluction processes can form small-scale lobes (Fig. 6b).

Analysing the spatial distribution of the negative values of the map (Fig. 3), three main zones were identified: i) the summit craters, ii) the 2001 and 2002–2003 cones, and iii) the Valle del Bove western portion. In the summit craters zone, we observe a slight lowering (3–4 m) in the northern portion of the NEC that includes part of the rim and flank. A relevant collapse (about 80 m) is evident inside the southeast portion of the Bocca Nuova and two enclosed depressions are visible in the west sector of the NSEC, indicating a lowering of around 7–8 m. In the second zone, identified by the 2001 and 2002–2003 cones, only the flanks exposed to East are affected by a lowering that ranges from 2 to 10 m, as well as the northeast flank of the nearby Mt. Frumento Supino (Fig. 3). In the third zone, Valle the Bove, the decrease in elevation characterizes scattered areas of limited extent (<5000 m^2) along the west side and on the southern bottom. The areas located on the flanks can be explained by the very high steepness and roughness of the flanks themselves that, in

specific climatic conditions, can favour frequent and intense erosion triggering isolated detachment or more complex landslides. This is well highlighted in the roughness map (Fig. 7) calculated by applying the Index of Riley et al. (1999) to the 2015 Pleiades DEM. In fact, in the map, the highest values of roughness are identified along the northern and western walls of the Valle del Bove, whereas the lower values are present in the scoriae cones (2001 cone, 2002 cones, Mt. Frumento delle Concazze, Mt. Simone, M.te Centenari and Mt. Supino) and the lava flows. Further and more detailed distinctions can be possible combining the roughness map with other typologies of data (Spinetti et al., 2009; Fornaciai et al., 2010). As regards the depressions visible at the bottom of the west flank, they can be explained by local transport and erosion due to the accumulation of snow in the colder season and the following melting in spring. Moreover, the limited depression areas close to Valle del Leone is also shaped by freeze and thaw cycle.

Lastly, examining zones lower than 1700 m a.s.l. outside of the Valle del Bove (north-west and north-east portions of the study area), the map in Fig. 3 shows some areas with a peculiar stippled pattern represented by positive and negative values. These values are due to the changes in height of the vegetation that exists in these areas.

5.3. Erupted products volumes

In order to estimate the total volume of the erupted products between 30 September 2005 and 28 July 2015, we have considered the areas where the map of difference in height results greater than 1.6 m excluding the zones covered by clouds or volcanic plumes (see black outlines in Fig. 3) and/or affected by growing vegetation (see 5.2 section). The volume calculation was performed on matrix data by multiplying the extent of the areas for the respective difference in elevation between 2015 and 2005. In detail, the formula used is the following:

$$V = \sum_i \Delta Z_i * \Delta x^2 \quad (2)$$

where Δx is the grid cell size and Δz_i is the height difference between the post- and pre-eruption surfaces for each pixel.

The result indicates that products erupted in ten years have a volume of 284.3±15.8 x10^6 m^3 with an uncertainty of 5.5% at 95% C.I. These products include lava flows and pyroclastic deposits covering a total area of 15.8 km^2. Our results have been compared with the volume data available in literature and reported in Table 1 where the data are referred to single or multiple eruptions occurred in the investigated period. The sum of the volumes reported in Table 1 (218.81x $10^6 m^3$) is 23% lower than the volume calculated in this study (284.3±15.8 x10^6 m^3). This is expected considering the lack or partial quantification of several products erupted during the 10 years and the different accuracy of the methods used to map and calculate the products' volumes. Consequently, we have compared our volume with those that cover very similar timeframes and are obtained by using equivalent methods to ours. Following these criteria, our result was compared with Ganci et al. (2018) that estimates a volume of 287±37 x10^6 m^3 for the July 2005 - December 2015 period. This estimation has good agreement within its error limits with our result, although it is obtained comparing a photogrammetric DEM at 1 m spatial resolution and a satellite derived DEM at 4 m spatial resolution. A more precise volume calculation with a significantly reduced error has been obtained when using two models with same spatial resolution and comparable accuracy, such as 2005 Lidar and 2015 Pleiades DSMs. In addition, the calculated volume allowed to derive a yearly average volume of erupted products equal to 28.4 x10^6 m^3/y, comparable to the previous annual rate of the 1993–2013 period (Bonaccorso and Calvari, 2013).

Four zones of particular interest have been identified in the map of differences in height that quantifies the most evident morphological changes during the ten years. These four zones are outlined and coded with numbers from 1 to 4 in the map itself (Fig. 3).

Zone 1 (yellow dashed outline, Fig. 3.) identifies the scoriae cones and the lava flow field formed during the sub-terminal eruption occurred in 2014 in the eastern flank of the NE Crater (Spina et al., 2017). This zone involves an area of 0.76 km^2 with a volume of products equal to 8.6±0.8 x10^6 m^3. In detail, the lava field has an average thickness of 11 m with more than 35 m near the active eruptive fractures, in the central portion of the lava field itself. The 2014 scoriae cone

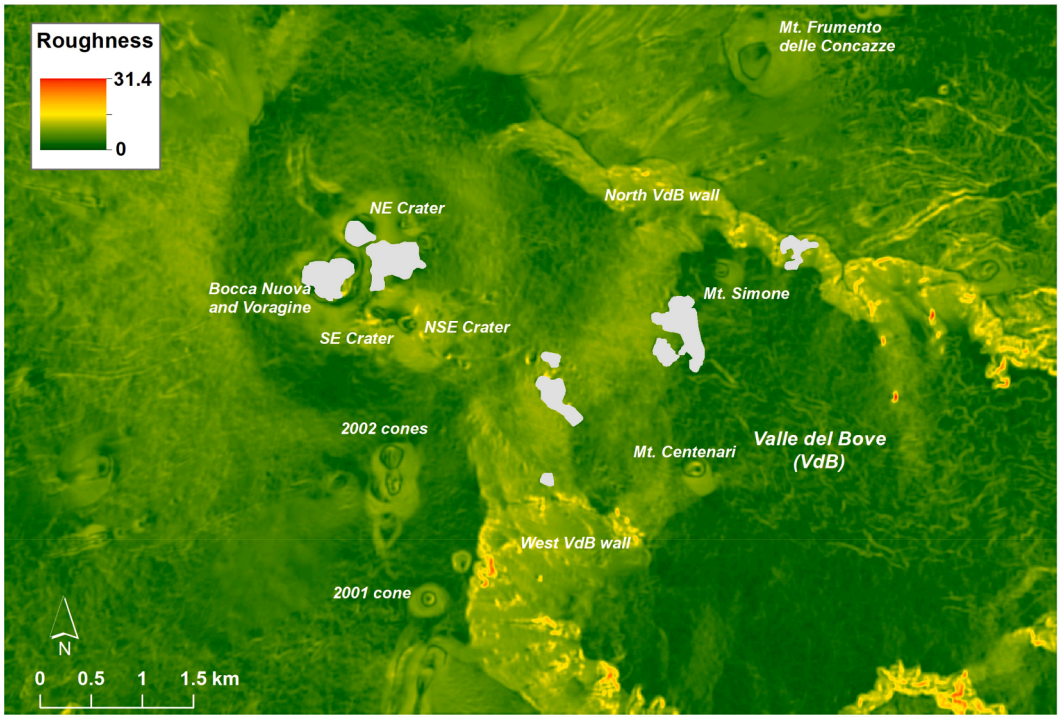

Fig. 7. 2015 Roughness map of the study area. The zones in grey mask the false morphologies generated by the presence of meteorological clouds, fumaroles and volcanic plume.

reaches the maximum height of 3142.7±0.8 m a.s.l. in the horseshoe cone located to the north. The calculated volume is greater than those estimated from De Beni et al. (2015) through field observations, and from Ganci et al. (2018) through thermal remote sensing. This is expected because both referred to only the lava flow field without taking into consideration the explosive products, which formed a scoriae cone around the eruptive vents.

Zone 2 (black dashed outline, Fig. 3) highlights the considerable increase of the SEC and NSEC cones due to the intense volcanic activity from July 2006 to May 2015. The volume of volcanic material that forms these cones was estimated at 53.7±0.7 x10^6 m^3 covering an area of 0.72 km^2. In particular, the NSEC represents the portion of the volcano where the products erupted in the ten years reached the highest thickness (210.7±1.6 m). Our volume (53.7±0.7 x10^6 m^3) has the same order of magnitude as the volumes estimated by Ganci et al. (2018) and Proietti et al. (2020) for the NSEC area only. However, both published estimations (55±1.5 x10^6 m^3 and 46 x10^6 m^3, respectively) do not allow a rigorous comparison with our volume because they referred only to the NSEC cone instead of the entire SEC-NSEC structure.

Zone 3 (red dashed outline in the map, Fig. 3) hosts a stratified lithology of alternating layers of lava and tephra fallout deposits. This zone covers an area of 1.29 km^2 and is situated in the highest portion of the south flank of Mt. Etna, between 2800 and 3000 m a.s.l., immediately below the SEC-NSEC apparatus. Here the lavas accumulated a maximum thickness of 20 m with a total volume of 10.1±1.3 x10^6 m^3. Such zone represents the most accessible area of Mt. Etna summit because it is easily reached by four-wheel drive buses that transport several thousand tourists each year.

Zone 4 (white dashed outline in the map, Fig. 3) defines the extent of the deposits accumulated on the upper portion of Valle del Bove. These deposits cover an area of 4.22 km^2 with a volume of volcanic material equal to 155.0±4.2 x10^6 m^3 that represents more than half of the total volume erupted by Mt. Etna in the investigated period.

Based on the calculated volumes above, the areas most exposed to volcanic activity are the cone-shaped structure generated by SEC and NSEC (zone 2) and the upper portion of Valle del Bove (zone 4). In particular, zone 2 is where the accumulation of pyroclastic deposits reaches the highest thickness (211 m) with a significant volume of 53.7±0.7 x10^6 m^3 represented by the SEC-NSEC structure, whereas the zone 4 represents the sector of the volcano mostly affected by effusive and explosive products and, in fact, it is characterized by the highest change in volume of 155.0±4.2 x10^6 m^3.

As mentioned previously, these quantifications do not consider the areas of no data, highlighted with black boundaries in Fig. 3. These areas of no data cover 1% of the entire study area. In particular 0.5% corresponds to crater degassing plume and the remaining 0.5% to the meteorological clouds and their shadows. Focusing the attention only on the thickness map, the meteorological clouds cover 2.3% of the entire map resulting in 1.6% of no data in the zone 4 (where the highest thickness has been identified).

Finally, the morphological changes occurred in the four zones have led a substantial modification of the drainage network as highlighted in Fig. 5. It shows that the 2015 drainage paths significantly change only in the areas covered by the products erupted in the investigated period. In fact, in these areas, 90% of the drainage networks routes are different. Such drainage network changes, strongly correlated with topography slope changes, may be able to modify the water direction runoff under extreme meteorological conditions, intensifying their natural flow towards the coastal municipality of Giarre that, with Riposto and Acireale, were affected by several disastrous floods in the past (Bisson et al., 2019).

6. Conclusions

This work maps the morphological changes of Mt. Etna volcano in the mid-upper portion from 2005 to 2015 and quantifies the relative total volume change with computed accuracy (RMSE <0.8 m). The results indicate that Mt. Etna, in ten years, emitted a products' volume of 284.3 x10^6 m^3 with an uncertainty of 5.5% at 95% C.I. This value is 23% higher than the sum of the volumes obtained for each occurred eruption and previously published in literature. This is expected considering the lack or partial quantification of several products erupted during the 10 years. Otherwise, the calculated volume is in agreement, within the reported errors, with a literature work referred to similar period and remote sensing technique. In addition, the yearly average volume of erupted products of 28.4 x10^6 m^3/y is comparable to the 1993–2013 annual rate previously estimated in literature.

The most relevant morphological changes refer to: i) the upper portion of the Valle del Bove, where the volume of the emitted products, 155 x10^6 m^3, represents more than half of all erupted volume in ten years (284.3 x10^6 m^3); ii) the birth of scoriae cones generated by the intense volcanic activity of the SEC and NSEC resulting in a products volume of 53.8 x10^6 m^3. These products reach the maximum thickness of all erupted deposits (211±1.6 m) in the south-east portion of the NSEC; iii) the formation of the scoriae cones and the lava flow field generated from the 2014 sub-terminal eruption on the eastern flank of the NEC. These products cover an area of 0.76 km^2 with a volume of 8.6 x10^6 m^3. This lava flow field is characterized by an average thickness of 11 m with a maximum of more than 35 m reached on the summit of the horseshoe cone and near the eruptive fractures positioned in the central portion of the lava field itself; iv) alternating layers of lava and tephra fallout deposits situated immediately below the SEC-NSEC apparatus (a touristic area). Here the accumulated volcanic products show a maximum thickness of 20 m and a volume of 8.6 x10^6 m^3.

Based on these observations, the areas most affected by the 2005–2015 volcanic activities are the upper portion of the Valle del Bove and the large structure generated by the intense activity of the SEC and NSEC cones. The rigorous methodology applied here allowed us to increase the accuracy of the calculated volume of the emitted products between 2005 and 2015, and to reduce by an order of magnitude the error estimation with respect to previously published results, irrespective of the methodologies employed (thermal, remote sensing, photogrammetric). Besides, without a rigorous analysis of errors, different sources of DEMs cannot be accurately compared, and change analysis results start to be meaningless. For this reason, our results, obtained with a narrower margin of error, represent an improved contribution to the topographic changes quantification in active volcanic areas allowing to derive more accurately key parameters often used in many volcanic hazard studies.

Declaration of Competing Interest

The authors declare that they have no known competing financial interests or personal relationships that could have appeared to influence the work reported in this paper.

Acknowledgments

We are grateful to ASTRIUM, Airbus Defense and Space for Pleiades data availability. In addition, we want to thank the two anonymous reviewers and Emily Montgomery-Brown for their very helpful suggestions.

References

Aloisi, M., Bonaccorso, A., Cannavò, F., Gambino, S., Mattia, M., Puglisi, G., Boschi, E., 2009. A new dike intrusion style for the Mount Etna May 2008 eruption modelled through continuous tilt and GPS data. Terra Nova 21 (4), 316–321. https://doi.org/10.1111/j.1365-3121.2009.00889.x.

Alparone, S., Andronico, D., Lodato, L., Sgroi, T., 2003. Relationship between tremor and volcanic activity during the Southeast Crater eruption on Mount Etna in early 2000. J. Geophys. Res. 108 (B5), 2241. https://doi.org/10.1029/2002JB001866.

Anderson, S.W., 2018. Uncertainty in quantitative analyses of topographic change: error propagation and the role of thresholding. Earth Surface Processes and Landforms 44, 1015–1033. https://doi.org/10.1002/esp.4551.

Andronico, D., Lodato, L., 2005. Effusive Activity at Mount Etna Volcano (Italy) During the 20th Century: A Contribution to Volcanic Hazard Assessment. Natural Hazards 36, 407–443. https://doi.org/10.1007/s11069-005-1938-2.

Andronico, D., Branca, S., Calvari, S., Burton, M., Caltabiano, T., Corsaro, R.A., Del Carlo, P., Garfì, G., Lodato, G., Miraglia, L., Murè, F., Neri, M., Pecora, E., Pompilio, M., Salerno, G., Spampinato, L., 2005. A multi-disciplinary study of the 2002–03 Etna eruption: insights into a complex plumbing system. Bull. Volcanol. 67, 314–330. https://doi.org/10.1007/s00445-004-0372-8.

Andronico, D., Scollo, S., Cristaldi, A., Caruso, S., 2008. The 2002–03 Etna explosive activity: tephra dispersal and features of the deposit. J. Geophys. Res. 113, B04209. https://doi.org/10.1029/2007JB005126.

Andronico, D., Scollo, S., Cristaldi, A., Ferrari, F., 2009a. Monitoring ash emission episodes at Mt. Etna: the 16 November 2006 case study. J. Volcanol. Geotherm. Res. 180 (2–4), 123–134. https://doi.org/10.1016/j.jvolgeores.2008.10.019.

Andronico, D., Spinetti, C., Cristaldi, A., Buongiorno, M.F., 2009b. Observations of Mt. Etna volcanic ash plumes in 2006: an integrated approach from ground-based and polar satellite NOAA-AVHRR monitoring system. J. Volcanol. Geotherm. Res. 180 (2–4), 135–147. https://doi.org/10.1016/j.jvolgeores.2008.11.013.

Andronico, D., Scollo, S., Cristaldi, A., Castro, M.D.L., 2014. Representivity of incompletely sampled fall deposits in estimating eruption source parameters: a test using the 12–13 January 2011 lava fountain deposit from Mt. Etna volcano, Italy. Bulletin of volcanology 76 (10), 1–14.

Andronico, D., Scollo, S., Cristaldi, A., 2015. Unexpected hazards from tephra fallouts at Mt Etna: the 23 November 2013 lava fountain. J. Volcanol. Geotherm. Res. 304, 118–125. https://doi.org/10.1016/j.jvolgeores.2015.08.007.

Andronico, D., Di Roberto, A., De Beni, E., Behncke, B., Bertagnini, A., Del Carlo, P., Pompilio, M., 2018a. Pyroclastic density currents at Etna volcano, Italy: The 11 February 2014 case study. J. Volcanol. Geotherm. Res. 357, 92–105. https://doi.org/10.1016/j.jvolgeores.2018.04.012.

Andronico, D., Behncke, B., De Beni, E., Cristaldi, A., Scollo, S., Lopez, M., Lo Castro, M. D., 2018b. Magma budget from lava and tephra volumes erupted during the 25–26 October 2013 lava fountain at Mt Etna. Frontiers in Earth Science 6, 116.

Axelsson, P., 1999. Processing of Laser Scanner Data – Algorithms and Applications. ISPRS Journal of Photogrammetry & Remote Sensing 54, 138–147.

Bailey, J.E., Harris, A.J., Dehn, J., Calvari, S., Rowland, S.K., 2006. The changing morphology of an open lava channel on Mt. Etna. Bulletin of volcanology 68 (6), 497–515.

Barberi, F., Carapezza, M.L., Valenza, M., Villari, L., 1993. The control of lava flow during the 1991–1992 eruption of Mt. Etna. Journal of volcanology and geothermal research 56 (1–2), 1–34.

Behncke, B., Neri, M., 2003. The July–August 2001 eruption of Mt. Etna (Sicily). Bulletin of Volcanology 65 (7), 461–476.

Behncke, B., Branca, S., Corsaro, R.A., De Beni, E., Miraglia, L., Proietti, C., 2014. The 2011–2012 summit activity of Mount Etna: Birth, growth and products of the new SE crater. Journal of Volcanology and Geothermal Research 270, 10–21.

Behncke, B., Fornaciai, A., Neri, M., Favalli, M., Ganci, G., Mazzarini, F., 2016. Lidar surveys reveal eruptive volumes and rates at Etna, 2007–2010. Geophys. Res. Lett. 43, 4270–4278. https://doi.org/10.1002/2016GL068495.

Beyer, R.A., Alexandrov, O., McMichael, S., 2018. The Ames Stereo Pipeline: NASA's open source software for deriving and processing terrain data. Earth and Space Science 5 (9), 537–548.

Bisson, M., Spinetti, C., Neri, M., Bonforte, A., 2016. Mt. Etna volcano high resolution topography: Airborne Lidar modelling validated by GPS data. Int. J. of Digital Earth 9, 7, 710–732.

Bisson, M., Neri, M., Spinetti, C., Stefanelli, P., Basile, G., Panebianco, M., 2019. Mt. Etna eastern flank flooding hazard: a first evaluation based on GIS approach. Rend. Online Soc. Geol. It. 48, 69–75. https://doi.org/10.3301/ROL.2019.40).

Bonaccorso, A., Bonforte, A., Calvari, S., Del Negro, C., Di Grazia, G., Ganci, G., Neri, M., Vicari, A., Boschi, E., 2011. The initial phases of the 2008–2009 Mount Etna eruption: A multidisciplinary approach for hazard assessment. J. Geophys. Res. 116, B03203. https://doi.org/10.1029/2010JB007906.

Bonaccorso, A., Calvari, S., 2013. Major effusive eruptions and recent lava fountains: Balance between expected and erupted magma volumes at Etna volcano. Geophysical Research Letters 40 (23), 6069–6073.

Bonforte, A., and. Puglisi G. (2006). Dynamics of the Eastern Flank of Mt. Etna Volcano (Italy) Investigated by a Dense GPS Network. Journal of Volcanology and Geothermal Research 153: 357–369. doi:10.1016/j.jvolgeores.2005.12.005.

Branca, S., Del Carlo, P., 2004. Eruptions of Mt Etna during the past 3.200 years: a revised compilation integrating the Historical and stratigraphic records. Mt. volcano laboratory. AGU, Etna.

Branca, S., Del Carlo, P., 2005. Types of eruptions of Etna volcano AD 1670–2003: implications for short-term eruptive behavior. Bull. Volcanol. 67, 732–742. https://doi.org/10.1007/s00445-005-0412-z.

Calvari, S., Coltelli, M., Neri, M., Pompilio, M., Scribano, V., 1994. The 1991–1993 Etna eruption: chronology and lava flow-field evolution. Acta Vulcanol. 4, 1–14.

Calvari, S., Pinkerton, H., 2004. Birth, growth and morphologic evolution of the 'Laghetto' cinder cone during the 2001 Etna eruption. Journal of Volcanology and Geothermal Research 132 (2–3), 225–239.

Cannavo, F., Sciotto, M., Cannata, A., Di Grazia, G., 2019. An integrated geophysical approach to track magma intrusion: The 2018 Christmas Eve eruption at Mount Etna. Geophysical Research Letters 46, 8009–8017. https://doi.org/10.1029/2019GL083120.INGV-OE, 2020. Bollettino settimanale sul monitoraggio vulcanico, geochimico e sismico del vulcano Etna. 23/11/2020 - 29/11/2020. Rep. No 49/2020. Available at http://www.ct.ingv.it/en/rapporti/multidisciplinari.html?view=docman.

Coltelli, M., Proietti, C., Branca, S., Marsella, M., Andronico, D., Lodato, L., 2007. Analysis of the 2001 lava flow eruption of Mt. Etna from three-dimensional mapping. J. Geophys. Res. 112, F02029. https://doi.org/10.1029/2006JF000598.

Corsaro, R.A., Andronico, D., Behncke, B., Branca, S., De Beni, E., Caltabiano, T., Ciancitto, F., Cristaldi, A., La Spina, A., Lodato, L., Giammanco, S., Miraglia, L., Neri, M., Salerno, G., Scollo, S., Spada, G., 2017. Monitoring the December 2015 summit eruptions of Mt. Etna (Italy): implications on eruptive dynamics. J. Volcanol. Geotherm. Res. 341, 53–69. https://doi.org/10.1016/j.jvolgeores.2017.04.018.

De Beni, E., Behncke, B., Branca, S., Nicolosi, I., Carluccio, R., Caracciolo D'Ajello, F., Chiappini, M., 2015. The continuing story of Etna's New Southeast Crater (2012–2014): evolution and volume calculations based on field surveys and aerophotogrammetry. J. Volcanol. Geotherm. Res. 303, 175–186.

De Beni, E., Cantarero, M., Messina, A., 2019. UAVs for volcano monitoring: A new approach applied on an active lava flow on Mt. Etna (Italy), during the 27 February–02 March 2017 eruption. Journal of Volcanology and Geothermal Research 369, 250–262.

Deilami, K., Hashim, M., 2011. Very high resolution optical satellites for DEM generation: A review. European Journal of Scientific Research 49 (4), 542–554.

Del Negro, C., Cappello, A., Ganci, G., 2016. Quantifying lava flow hazards in response to effusive eruption. GSA Bulletin 128 (5/6), 752–763. https://doi.org/10.1130/B31364.1.

Di Grazia, G., Cannata, A., Montalto, P., Patanè, D., Privitera, E., Zuccarello, L., Boschi, E., 2009. A multiparameter approach to volcano monitoring based on 4D analyses of seismo-volcanic and acoustic signals: The 2008 Mt. Etna eruption. Geophys. Res. Lett. 36, L18307. https://doi.org/10.1029/2009GL039567.

Etzelmuller, B., 2000. On the quantification of surface changes using grid-based digital elevation models. Transactions in GIS 4 (2), 129–143. https://doi.org/10.1111/1467-9671.00043.

Fornaciai, A., Bisson, M., Landi, P., Mazzarini, F., Pareschi, M.T., 2010. A LiDAR survey of Stromboli volcano (Italy): Digital elevation model-based geomorphology and intensity analysis. International Journal of Remote Sensing 31 (12), 3177–3194.

Fornaciai, A., Andronico, D., Favalli, M., Spampinato, L., Branca, S., Lodato, L., Bonforte, A., Nannipieri, L., et al., 2021. The 2004-05 Mt. Etna compound lava flow field: a retrospective analysis by combining remote and field methods. J. Geophys. Res. - Solid Earth 126. https://doi.org/10.1029/2020JB020499.

Ganci, G., Cappello, A., Bilotta, G., Herault, A., Zago, V., Del Negro, C., 2018. Mapping volcanic deposits of the 2011–2015 Etna eruptive events using satellite remote sensing. Frontiers in Earth Science 6, 83.

Harris, A.J.L., Blake, S., Rothery, D.A., Stevens, N.F., 1997. A chronology of the 1991 to 1993 Mount Etna eruption using advanced very high resolution radiometer data: Implications for real-time thermal volcano monitoring. J. Geophys. Res. 102, 7985–8003.

Harris, A.J.L., Flynn, L.P., Keszthelyi, L., Mouginis-Mark, P.J., Rowland, S.K., Resing, J. A., 1998. Calculation of lava effusion rates from Landsat TM data. Bull Volcanol 60, 52–71.

Harris, A.J.L., Steffke, A., Calvari, S., Spampinato, L., 2011. Thirty years of satellite-derived lava discharge rates at Etna: Implications for steady volumetric output. J. Geophys. Res. 116, B08204. https://doi.org/10.1029/2011JB008237.

Harris, A.J.L., Steffke, A., Calvari, S., Spampinato, L., 2012. Correction to "Thirty years of satellite-derived lava discharge rates at Etna: Implications for steady volumetric output". J. Geophys. Res 117, B08207.

INGV-OE, 2014. Bollettino settimanale sul monitoraggio vulcanico, geochimico e sismico del vulcano Etna. 22/12/2014 - 28/12/2014. Rep. N° 01/2015. Available at http://www.ct.ingv.it/en/rapporti/multidisciplinari.html?view=docman.

INGV-OE, 2015a. Bollettino settimanale sul monitoraggio vulcanico, geochimico e sismico del vulcano Etna. 26/01/2015 - 01/02/2015. Rep. N° 06/2015. Available at http://www.ct.ingv.it/en/rapporti/multidisciplinari.html?view=docman.

INGV-OE, 2015b. Bollettino settimanale sul monitoraggio vulcanico, geochimico e sismico del vulcano Etna. 11/05/2015 - 17/05/2015. Rep. N° 21/2015. Available at http://www.ct.ingv.it/en/rapporti/multidisciplinari.html?view=docman.

Laiolo, M., Ripepe, M., Cigolini, C., Coppola, D., Della, S.M., Genco, R., Innocenti, L., Lacanna, G., Marchetti, E., Massimetti, F., Silengo, M.C. (2019). Space- and ground-based geophysical data tracking of magma migration in shallow feeding system of Mount Etna volcano. Remote Sensing, 11, 1182, Special Issue "Remote Sensing of Volcanic Processes and Risk". doi:org/10.3390/rs11101182.

Lombardo, V., Silvestri, M., & Spinetti, C. (2011). Near real-time routine for volcano monitoring using infrared satellite data. Annals of geophysics.

Lombardo, V., Pick, L., Spinetti, C., Tadeucci, J., Zakšek, K., 2020. Temperature and Emissivity Separation 'Draping'Algorithm Applied to Hyperspectral Infrared Data. Remote Sensing 12 (12), 2046.

Neri, M., Mazzarini, F., Tarquini, S., Bisson, M., Isola, I., Behncke, B., Pareschi, M.T., 2008. The changing face of Mount Etna's summit area documented with Lidar technology. Geophysical Research Letters 35 (9).

Palaseanu-Lovejoy, M., Bisson, M., Spinetti, C., Buongiorno, M.F., Alexandrov, O., Cecere, T., 2019. High-Resolution and Accurate Topography Reconstruction of Mount Etna from Pleiades Satellite Data. Remote Sensing 11 (24), 2983.

Poret, M., Costa, A., Andronico, D., Scollo, S., Gouhier, M., Cristaldi, A., 2018. Modeling eruption source parameters by integrating field, ground-based, and satellite-based measurements: The case of the 23 February 2013 Etna paroxysm. J. Geophys. Res.-Solid. Earth 123. https://doi.org/10.1029/2017JB015163.

Proietti, C., Coltelli, M., Marsella, M., Martino, M., Scifoni, S., Giannone, F., 2020. Towards a satellite-based approach to measure eruptive volumes at Mt. Etna using Pleiades datasets. Bulletin of Volcanology 82 (4), 1–15.

Riley, S. J., DeGloria, S. D., & Elliot, R. (1999). Index that quantifies topographic heterogeneity. intermountain Journal of sciences, 5(1-4), 23-27.

Spina, L., Taddeucci, J., Cannata, A., Sciotto, M., Del Bello, E., Scarlato, P., Kueppers, U., Andronico, D., Privitera, E., Ricci, T., Pena-Fernandez, J., Sesterhenn, J., Dingwell, D.B., 2017. Time-series analysis of fissure-fed multi-vent activity: a snapshot from the July 2014 eruption of Etna volcano (Italy). Bull. Volcanol. 79, 51. https://doi.org/10.1007/s00445-017-1132-x.

Spinetti, C., Mazzarini, F., Casacchia, R., Colini, L., Neri, M., Behncke, B., Pareschi, M.T., 2009. Spectral properties of volcanic materials from hyperspectral field and satellite data compared with LiDAR data at Mt. Etna. International Journal of Applied Earth Observation and Geoinformation 11 (2), 142–155.